Synthesis and Physicochemical Properties of Polyamideimide Membranes Containing ZIF-8 and CMS Particles for Potential Gas Separation Applications

Sasikumar Balaguru
NIT-Trichy: National Institute of Technology Tiruchirappalli
Yohannan Subin Sabilon
NIT-Trichy: National Institute of Technology Tiruchirappalli
Arthanareeswaran Gangasalam (arthanaree10@yahoo.com)
National Institute of Technology Tiruchirappalli

Research Article

Keywords: Carbon molecular sieves, Zeolitic imidazolate frameworks 8, Gas separation, Polyamideimide, Membranes

Posted Date: October 29th, 2021

DOI: https://doi.org/10.21203/rs.3.rs-974735/v1

Abstract

The present study involves the fabrication and characterization of Polyamideimide (PAI) membrane holding ZIF-8 and CMS particles for potential gas separation applications. Zeolitic imidazolate frameworks-8 (ZIF-8) nanocrystals were prepared by a precipitation reaction with Zinc metal cluster and 2-methylimidazole, whereas the carbon molecular sieves (CMS) were synthesized by pyrolysis of polyamideimide (PAI) polymer. ZIF-8 and CMS particles were characterized comprehensively for the functional group, crystallinity, and morphological analyses. The successful formation of ZIF-8 nanocrystals was evident from the rhombic octahedron shape, and EDX confirms the presence of Zn metal cluster and methylimidazole linker. The ZIF-8 and CMS nanoparticles incorporated PAI membranes were prepared using phase inversion technique with varying loading wt.% of 1, 2, and 3%. PAI/ZIF-8 and PAI/CMS membranes cross-sectional morphology confirmed that synthesized nanoparticles were well embedded through the PAI membrane. The PAI/ZIF-8 (3 %) membrane, thin dense skin top layer, and well-defined honeycomb porous substructure were observed. Furthermore, the ZIF-8 and CMS particles incorporation have a beneficial impact on the mechanical properties of PAI at the low loading of nanoparticles. Thus, the inclusion of ZIF-8 and CMS particles in the PAI matrix positively altered the physicochemical properties of the resulting hybrid membranes, which could help them achieve remarkable gas permeance and selectivity.

1. Introduction

The effective CO_2 separation from other light gases is a crucial environmental challenge that has been extensively studied in recent years. The imminent climate change issues associated with the increasing concentration of anthrophonic CO_2 led to the importance of CO_2 separation (Taheri and Raisi 2021). The hydrogen production using a water shift gas reaction produces CO and CO_2 as a by-product. Furthermore, CO_2 is a component of natural and biogas. So, it is essential for CO_2 capture from gas streams for fuels with improved energy content and reduces the climatic impact of CO_2 gas. Conventional technologies like adsorption, cryogenic distillation, and absorption were high energy-intensive processes, whereas membrane separation proved to be a promising energy-efficient technology for CO_2 separation (Xie et al. 2019).

Membrane gas separations have drawn attention over the years due to it lower cost and low energy requirement. Mixed matrix membranes (MMMs) are a combination of filler nanoparticle dispersed phase and polymers continuous phase (Cheng et al. 2019). The combination of higher permeability and selectivity with desired membrane stability of membranes are essential for gas separation. Although MMMs have a great future in gas separations, vital problems are the uniform dispersion at high filler content and mainly the attachment between heterogeneous phases. The functionalization of the filler surface and the use of additives can overcome both problems (Aroon et al. 2010). Another aspect of interest is the long-term stability of MMMs. In most glassy polymers, the filler inclusion can also help control the polymer relaxation, which results in a decline in the rate of permeation over time (Goh et al.

2011). Robeson, in early 1990, anticipated an upper limit for the working efficiency of polymeric membranes in gas separation (Robeson 2008; Zhang et al. 2013). MMMs can achieve more excellent permeance and selectivity, or both concerning the existing polymeric materials, due to the inclusion of the inorganic fillers with their built-in remarkable separation properties (Chung et al. 2007; Ismail et al. 2009).

ZIFs, a subclass of metal-organic frameworks (MOFs), offer diverse structures, higher surface area, and tunable pore size. ZIFs proved to be a promising material for fillers in polymeric matrices because of their sorption and separation of gases and vapors properties. ZIFs are proving as potential material to improve the performance of membranes to overcome the Robeson bound. The advantage of incorporating ZIFs into the polymer matrix over non-porous materials is that their organic components enhance the interfacial compatibility with the polymer matrices. ZIF-8 has a sodalite topology with exceptional CO_2 affinity with better mechanical and thermal stability. Ordoñez et al. reported a significant enhancement in gas permeability even at higher filler loading (40 wt%) with the absence of interfacial voids because of the unique properties of ZIF-8 (Ordoñez et al. 2010). Dai et al. obtained a 20% increase in selectivity of CO_2/N_2 using 17 vol % of ZIF-8 in the selective skin layer compared to neat Ultem® membranes (Dai et al. 2012). Nordin et al. investigated the performance of ZIF-8 with 0.5 wt.% loading on flat sheet membranes using PSf as membrane matrix (Nordin et al. 2015), and it has found that the CO_2/CH_4 selectivities were enhanced by 19 % compared to the neat membrane. CMS is derived from the pyrolysis of polymeric precursors having well-defined microporous structures that could separate gas pairs based on molecular sieving properties and thus exhibit higher gas permeability and selectivity. Koros et al. synthesized two CMS hollow fibers using Matrimid-5218 and 6FDA/BPDA-DAM as precursors for CO_2/CH_4 separation. Both CMS fibers have shown different permeation results under similar conditions.

Furthermore, the CMS fibers properties can be varied by varying the parameter, namely temperature, thermal soak time, etc. (Vu et al. 2002). MMMs with CMS showed a 19% increase in CO_2/CH_4 selectivities than pure matrimid polymer film (Vu et al. 2003a). This shows that CMS particles could be a promising material to enhance the performance of MMMs for gas separation applications. Herein, we report the synthesis of ZIF-8 nanocrystals and CMS particles to fabricate PAI-based MMMs for potential gas separation applications.

2. Materials And Methods

2.1 Materials

Zinc hydrate crystals were procured from Merck, India. Sigma Aldrich has supplied 2-methylimidazole and n-butylamine. PAI polymer was purchased from Solvay specialty polymer, India. Merck, India also supplied acetone and methanol.

2.2 Experimental

2.2.1 ZIF-8 nanocrystals synthesis

For ZIF-8 nanocrystal synthesis, two solutions, one of 2.469 mmol, Zn $(NO_3)_2 \cdot 6H_2O$ crystals, were dissolved completely in 50 ml methanol under constant magnetic stirring 9.874 mmol, 2-methylimidazole (Hmim) in 50 mL of methanol were prepared separately. Furthermore, the modulator n-butylamine was added to the later solution to control the crystal particle size. The solution containing organic ligand 2-methylimidazole (Hmim) was mixed to the other under constant stirring and the solution aged for 24h at 30°C. The resultant white powder was filtered using centrifugation at 10000 rpm, washed with methanol, and dried. The resulting white powder is finely grounded and stored in the desiccator for further characterization (Maya et al. 2015).

2.2.2 Synthesis of CMS particles

The CMS particles was synthesized using PAI as the polymer matrix by solution casting technique. The predetermined PAI polymer was added into 25ml NMP solvent in a Scott bottle under constant magnetic stirring. Then the PAI polymer solution was allowed to stand still for 24 h at 30°C to release the bubbles from the dope solution. Further, the solution was poured onto a glass plate, and then it was cast using a thin-film applicator with 750 μm thickness. Furthermore, the casted membrane was dried at 30°C overnight for solvent evaporation. The PAI membrane was kept in the tubular furnace for pyrolysis at a specific temperature profile (Vu et al. 2002, 2003b) and under an N_2 environment. After pyrolysis, the CMS particles so formed were grounded into fine powder. The confirmation of these CMS particles was done using XRD analysis.

2.2.3 Fabrication of ZIF-8 and CMS nanoparticles incorporated PAI hybrid membranes

A series of ZIF-8 and CMS filler particles incorporated PAI asymmetric composite membranes were fabricated with 1, 2, and 3 wt. % loading using dry phase inversion method. The detailed composition of ZIF-8 and CMS filler dope solution was displayed in Table 1 **and** Table 2, respectively. The predetermined ZIF-8 and CMS particles were added separately to NMP solvent and stirred for 20 mins under a magnetic stirrer. Furthermore, the complete dispersion of filler particles was ensured by the sonication for 60 min. The filler suspension was then subjected to priming technique to ensure the optimum wetting and make the particle more compatible with the bulk polymer film to promote the affinity between the filler and the PAI polymer matrices. Initially, 1/10th of the PAI polymers were added, and it was kept under magnetic stirring at 60°C for 3 h. Then, the remaining PAI polymers were mixed and stirred until the complete dissolution.

Table 1
Composition of PAI/ZIF-8 membranes

Membranes	PAI polymer (%)	ZIF-8 (%)	Solvent NMP (%)
PAI/ZIF-8 (1 %)	16.5	1	82.5
PAI/ZIF-8 (2 %)	15.5	2	82.5
PAI/ZIF-8 (3 %)	14.5	3	82.5

Table 2
Composition of PAI/CMS membranes

Membranes	PAI polymer (%)	CMS (%)	Solvent NMP (%)
PAI/CMS (1 %)	16.5	1	82.5
PAI/CMS (2 %)	15.5	2	82.5
PAI/CMS (3 %)	14.5	3	82.5

Furthermore, the solution was allowed degassed at room temperature overnight. A prepared dope solution was poured into a flat glass plate and cast using a thin-film applicator with 750 µm thickness. Finally, the casted membranes were allowed to dry to 35°C for 24 h for the complete evaporation of NMP solvent, and the fabricated membranes were stored in a desiccator for further characterization.

2.2.3 Materials and membrane characterization:

The UV Vis absorption spectroscopy was used for the ZIF-8 nanocrystals confirmation. ZIF-8 and CMS fillers particles crystallinity was investigated using XRD (Perkin Elmer, USA) at 40 kV and 30 mA in the 2θ scanning range. The surface morphology of ZIF-8 particles, PAI/ZIF-8, and PAI/CMS membranes was investigated using FESEM (JSM-6701F, JOEL). Furthermore, the surface morphology of the ZIF-8 filler particles was also analyzed using a TEM (JEM 2100, JOEL, Japan). The film elemental analysis to confirm the carbon presence of carbon was conducted by utilizing EDX with a magnification of 3000× and 15 kV voltage. The functional group analysis of fabricated PAI/ZIF-8 and PAI/CMS MMMs and ZIF-8 particles were confirmed using FTIR (Thermo scientific Nicolet iS5, USA) in the range of 4000 and 400 cm^{-1}. The mechanical properties of PAI/ZIF-8 and PAI/CMS membranes were investigated using a tensile strength analyzer (INSTRON 4500, UK) as per the ASTM D882 standards at room temperature. The experiments were performed three times, and the average values were presented. The hydrophilicity and porosity of the membranes were determined using the procedure as reported earlier in the literature (Aditya Kiran et al. 2016).

3. Results And Discussion

3.1 UV visible spectroscopy and crystallinity of ZIF-8:

The UV Visible spectroscopy analysis of ZIF-8 nanocrystals were illustrated in Figure 1. The penetration was proportionate to excitation wavelength, i.e., 325 nm, due to the decrease in absorbance. The presence of an absorption peak at 325 nm confirms the ZIF-8 nanocrystal formation (Liu et al. 2013).

The crystallinity of ZIF-8 nanocrystals was studied using XRD techniques, and their corresponding XRD patterns were illustrated in Figure 2. The instantaneous solid formation was observed with the inclusion of n-butylamine as a modulating ligand, and the ZIF-8 crystals were recovered from the solution after 24 h (Pan et al. 2011). The strong characteristic peaks around 18° confirm the successful formation of ZIF-8 nanocrystals (Cravillon et al. 2011). The average size of particles was noted to be about 18 nm.

3.2 Chemical structure and thermal properties of ZIF-8:

The functional group analysis of ZIF-8 nanocrystals was studied using FTIR techniques, and their corresponding spectra were illustrated in Figure 3. Several bands were observed between 400-2000 cm^{-1}. The main bands that characterized the ZIF-8 were shown at 1148 and 763 cm^{-1}, ascribed to C=N and C-N stretching, respectively (Anastasiou et al. 2016). The absorption bands at 2929 and 3137 cm^{-1} correspond to the aromatic and aliphatic C-H imidazole stretch bands. The peak at 1579 cm^{-1} corresponds to the C=N stretching, and absorption bands at 420 cm^{-1} were noted for the Zn-N stretching mode. Besides, the peaks at 1100-1400 cm^{-1} (C-N stretching), confirming the successful formation of ZIF-8 nanocrystals (Liu et al. 2016). The thermal stability of the ZIF-8 nanocrystals was characterized using TGA analysis and presented in Figure 4. The synthesized ZIF-8 nanocrystals were highly thermally stable, and it is started to decomposition after 520°C due to the 2-methylimidazole, and it can enable to work on high gas separation applications when we incorporate them into the membrane matrix (Sasikumar et al. 2021).

3.3 Surface morphology of ZIF-8 nanocrystals

The ZIF-8 has theoretical cavities of 11.6 Å connected by 3.4 Å aperture size, making them suitable materials to be used membranes to enhance the molecular sieving properties (Sorribas et al. 2014). The performance of ZIF-8 nanomaterials depends mainly on their size, shape, and well-defined porous nature (Cravillon et al. 2011). The surface morphology of ZIF-8 (Figure 5) displayed nanocrystals with a rhombic dodecahedral shape crystal structure (Pan et al. 2011; Liu et al. 2013). The EDX spectra of ZIF-8 nanocrystal were displayed in Figure 5, and their corresponding elemental composition was also presented in Table 3. The EDX spectra confirm the presence of C, N, O along with Zn. In addition, the ZIF-8 nanocrystals were also investigated using TEM analysis, and it is illustrated in Figure 6. The roughly spherical particles with sharp edges were observed in TEM images with a particle size of <100 nm.

Table 3
Elemental composition of ZIF-8 nanocrystals

S. No	Elements	Weight (%)	Atomic (%)
1.	Carbon	49.68	61.82
2.	Nitrogen	27.48	11.75
3.	Zinc	17.69	1.50
4.	Oxygen	5.16	2.79

Table 4
Elemental composition of CMS membrane

S. No	Element	Weight (%)	Atomic (%)
1.	Carbon	23.61	36.45
2.	Oxygen	27.46	31.82
3.	Sodium	3.22	2.60
4.	Aluminium	12.67	8.70
5.	Silicon	26.03	17.19
6.	Calcium	7.01	3.24

3.4 Confirmation of CMS particles

The synthesized CMS films were finely grounded into powders for use in mixed matrix membrane fabrications. It is desirable to ensure the permeation capability of CMS particles is comparable with the CMS films. However, it is tough to determine particles permeation properties like CMS films (Vu et al. 2003b). So the XRD diffractograms were done for CMS films and powders, as shown in Figure 7. The powder and film CMS displayed analogous d-spacings and peaks indicating the amid planar dimensions among powder and film pyrolyzed CMS particles, indicating CMS's successful synthesis (Vu et al. 2002, 2003b).

3.5 Surface morphology of CMS membrane

CMS membranes inherent CO_2/CH_4 selectivities were 200 and CO_2 permeability of 44 Barrers (Vu et al. 2003b). The significant enhancement of about 45% CO_2/CH_4 selectivities was reported for Matrimid®–CMS mixed matrix membranes. The top surface morphology of CMS was displayed in Figure 8a, and their corresponding EDX spectra were illustrated in Figure 8b. The presence of carbon peaks with the wt.% of 4.40 confirms the formation of CMS polymer films, whereas the sharp Si peak corresponds to the Si detector used during EDX analysis. Besides, the Oxygen peaks due to the oxygen atmosphere during the EDX.

3.6 Morphology of PAI/CMS membranes

The cross-sectional morphology of CMS incorporated PAI membranes were presented in Figure 8. The morphology of PAI/CMS (1%), PAI/CMS (2%), and PAI/CMS (3%) MMMs looks similar with the increase in loading wt% of CMS particles into the PAI matrix. However, the thickness of the top surface layer was found to be different from each other. The PAI precursor has a thin skin dense (1000-2000 Å) layer on a porous core, whereas the membrane cross-section showed a transition from the inner porous cores to the dense outer structure (Vu et al. 2003b). However, the CMS particle's surface incorporated PAI membranes showed a very dense structure without any interfacial defects, indicating the excellent compatibility between the PAI matrix and CMS particles. The presence of CMS particles is expected to offer better permeance of CO_2, CO_2/H_2, and CO_2/CH_4 selectivities of gas pairs (Vu et al. 2002, 2003c, a).

3.7 Morphology of PAI/ZIF-8 membranes

The cross-sectional morphology of PAI/ZIF-8 (1%), PAI/ZIF-8 (2%), and PAI/ZIF-8 (3%) membranes were illustrated in Figure 10. The asymmetric structure was observed with a thin dense skin layer followed by a porous sublayer. The thin dense layer indicates the good adhesion of bare ZIF-8 to the PAI matrix (Zhang et al. 2012). The synthesized ZIF-8 nanocrystals have shown good intimate contact with the PAI polymer without any modification, and this could be because of the ZIF-8 hydrophobic nature (Zhang et al. 2014).

Interestingly, the PAI/ZIF-8 membrane morphology was quite different compared to PAI/CMS membranes. With the increase in loading wt.% of ZIF-8, a large array of non-ideal crystals from 50 to several microns were observed. The larger size ZIF-8 particles (> 50 nm) were also observed along with the uniformly dispersed ZIF-8 nanocrystals with the increase in loading wt.%. However, the surface of these ZIF-8 large arrays looks smooth (Figure 10) without aggregation, and approximately no defects were seen in the PAI/ZIF-8 membrane. It is essential to get the uniform dispersion of ZIF-8 nanocrystals within the polymer matrix to achieved desired gas separation results. A better understanding of the formation of larger size ZIF-8 cluster formations and the impact on gas transport characteristics of the MMMs is required to further extend the asymmetric membranes for practical gas separation applications. The incorporation of ZIF-8 in the PAI membranes increases the thermal and chemical stability and gas separation performance of membranes (Keskin and Sholl 2009; Cravillon et al. 2011). Furthermore, the ZIF-8 as a filler nanocrystal would be expected to offer quadrupole moments of CO_2 and the electrostatic field of ZIF-8, which resulted in enhanced CO_2/CH_4 selectivities. Also, the ZIF-8 contributes to the increase in solubility of CO_2 due to its electrostatic interaction between the Zn metal and CO_2 molecules (Meshkat et al. 2020).

3.8 Functional group analysis PAI/ZIF-8 membranes

The functional group analysis of PAI/ZIF-8 membranes was investigated using FTIR, and their corresponding spectra were presented in Figure 11. The characteristic peaks of PAI polymer were observed at 3506 cm^{-1} (-NH), 1717 cm^{-1} (-CO) groups. The FTIR results shown in Figure 11 indicates the presence of aluminosilicates in the PAI/ZIF-8 membranes confirms the inclusion of ZIF-8 nanocrystals. Besides, the presence of ester, dimer, conjugated cyclic bond, and enols confirm due to the PAI polymer matrix (Rajesh et al. 2012). It can also be noted that with the loading percentage increases, the

transmittance value also increases, and this shows us that as the loading concentration of the inorganic filler increases, the permeability of the membranes increases.

3.9 Functional group analysis of PAI/CMS membranes

The chemical structure of PAI/CMS membranes was investigated using FTIR techniques, and their corresponding spectra were presented in Figure 12. The characteristic peaks of PAI polymer were observed at 3506 cm^{-1} attributed to the -NH amide linkage and the peaks at 1653 and 1717 cm^{-1} correspond to -CO stretching of amide linkage and stretching vibration of the five-member ring. With the increase in loading wt.% of CMS particles, the transmittance peaks were increased slightly, improving free volume in the membrane matrix. The presence of a carbon bond was observed at 1660 cm^{-1} (C=O bond) of carbon material, confirming the presence of CMS particles in the membrane matrix. The presence of CMS shows bands at 3228 cm^{-1} corresponding O-H stretching and the peaks at 2915 cm^{-1} assigned to C-H stretching. In addition, the 1576 cm^{-1} peak belongs to the carboxyl group (C=O). Furthermore, the presence of ester, dimer, conjugates cyclic bonds, and enols confirm the PAI polymer backbone and the band at 1000 were due to the O-H bending (El-Sheikh 2016). Furthermore, with the increase in loading wt%, there increase in transmittance %, which is expected to offer increased gas permeability. The CMS nanoparticles have proven to offer good selectivity and permeability. The CMS with rigid and well-defined pore structures is ideal for high pressure and temperature separation applications like hydrogen purification (Lei et al. 2021). Comparing FTIR results of both ZIF 8/PAI and CMS/PAI membranes shows that 3% ZIF 8/PAI has a maximum transmittance value of 95 while 3% CMS/PAI has a maximum transmittance value of 98.

3.10 Mechanical properties of PAI/ZIF-8 and PAI/CMS membranes

The mechanical strength of the ZIF-8 and CMS incorporated PAI membranes were studied using tensile study with the help of a universal tensile testing machine, and the values were displayed in Table 5. In the case of PAI/ZIF-8 (1 %), the yield ultimate stress and % elongation was found to be 2.58 MPa and 8.25 %, respectively. However, with the increase in loading percentage of ZIF-8 nanocrystal, the ultimate stress and % elongation was found to be decreasing. At 2 wt. % loading of ZIF-8 nanocrystals, the ultimate strain was noted to be 77.69% lower than the PAI/ZIF-8 (1%). The decrease in mechanical stability could be due to the agglomeration of ZIF-8 nanocrystal at a higher filler loading percentage. In the case of PAI/ZIF-8 (3 %), the membrane was very brittles that tensile test couldn't perform due to the aggregation of nanocrystals. Besides, in PAI/CMS (1%), the tensile stress was 5.41 MPa, whereas, in the PAI/CMS (3%) membrane, the stress was comparatively less. This shows that the stability of the membranes could decrease at the higher filler loading due to the aggregation of filler nanoparticles. Comparing the mechanical stability of PAI/ZIF-8 and PAI/CMS membranes shows that 1% PAI/ZIF-8 can endure a strain of 8.25%, whereas 1% PAI/CMS of about 3.72%. This could be due to the excellent adhesion and uniform dispersion of ZIF-8 nanocrystals at low loading weight because of the MOF structure. The increase in filler loading percentage in the membranes decreased the amount of force that the membrane

withstands. However, the increase in the filler loading percentage is expected to increase their permeability and selectivity values. Therefore, optimizing the loading wt.% of filler nanoparticles in the membrane matrix is crucial for potential gas separation applications.

Table 5
Mechanical stability of PAI/CMS and ZIF-8/PAI membranes

Membrane samples	Break Distance (mm)	Ultimate force (N)	% Total Elongation	Ultimate Stress (MPa)	Yield Stress (MPa)	Ultimate Strain (%)
PAI/CMS (1%)	1.79	24.3	8.95	5.41	5.41	3.72
PAI/CMS (2%)	1.62	23	8.08	5.10	0.0444	4.89
PAI/CMS (3%)	2.98	12.1	14.9	2.69	0.0118	3.87
PAI/ZIF-8 (1%)	1.75	11.6	8.77	2.58	0.00741	8.25
PAI/ZIF-8 (2%)	0.684	4.43	3.42	0.985	0.0148	1.84
PAI/ZIF-8 (3%)	-	-	-	-	-	-

Table 6
Water content and porosity of PAI/ZIF-8 and PAI/CMS membranes

Membranes	Filler (%)	Wet weight of the membrane (g)	Dry weight of the membrane (g)	Amount of water absorbed (g)	Porosity (nm)
PAI/ZIF-8 (1%)	1	0.0225	0.0079	0.0146	0.686
PAI/ZIF-8 (2%)	2	0.0300	0.0105	0.0195	0.687
PAI/ZIF-8 (3%)	3	0.0378	0.0130	0.0248	0.693
PAI/CMS (1%)	1	0.0068	0.0055	0.0013	0.219
PAI/CMS (2%)	2	0.0120	0.0100	0.0020	0.191
PAI/CMS (3%)	3	0.0178	0.0150	0.0028	0.181

3.11 Water content and porosity determination test

The effect of humid conditions during the gas separation measurements plays a crucial role in membranes performance. So, the water holding capacity and porosity determine the effectiveness of the membranes. The results of the tests are given in Table 3. In PAI/CMS membranes, the amount of water absorbed increases with the increase in CMS loading percentage. This is due to the hydrophilic property of the CMS nanoparticles that are present. This enhanced water retention property is expected to offer increased CO_2 permeance of the membranes. The incorporated ZIF-8 and CMS increase the free volume in the membrane matrix, which significantly increases the permeability. Therefore, these membranes can withstand fouling for a longer period due to their hydrophilic property. PAI/ZIF-8 membranes also followed a similar trend. Comparing the amount of water absorption of PAI/ZIF-8 and PAI/CMS membranes shows that 1% PAI/ZIF-8 can absorb 0.0146g of water while 1% CMS/PAI can absorb 0.0013g of water. So, compared to the amount of water absorbed, PAI/ZIF-8 membranes are more hydrophilic than PAI/CMS membranes. Also, as the concentration of the ZIF-8 increases, the porosity of the PAI/ZIF-8 membranes increases slightly due to the ZIF-8 structure. This phenomenon increases the permeability of the membranes as the porosity of the PAI/ZIF-8 membranes increases, thereby offering good CO_2/H_2 gas separation. On the other hand, the porosity of the PAI/CMS membranes keeps on decreasing as the concentration of CMS nanoparticles in the membrane increases. This may be due to the agglomeration caused due to the increase in the concentration of CMS particles which leads to a decrease in the permeability of the CMS/PAI membranes for gas separation. The increase in membrane water absorption capacity is expected to offer better fouling resistance.

4. Conclusion

A series of ZIF-8 and CMS particles incorporated PAI membranes were fabricated using dry- phase inversion technique for potential gas separation applications. The ZIF-8 and CMS particles were synthesized and characterized using FTIR, XRD, and TGA techniques. The functional group analysis and crystalline study confirming the formation of ZIF-8 nanocrystal. The morphological studies of ZIF-8 support evidence for forming rhombic dodecahedral crystals with a particle size of around 100 nm. Thermal studies of ZIF-8 nanocrystals have also shown thermal stability up to 500°C; proving can be applied for high-temperature gas separation applications, whereas the formation of CMS from the pyrolysis of PAI polymer was confirmed with the help of XRD spectra. Further, the effect of varying loading percentages of ZIF-8 and CMS particles on the PAI membrane matrix physicochemical properties were investigated for possible usage in gas separation applications. Cross-section morphology revealed that the ZIF-8 and CMS particles addition has a dominant effect on the internal and porosity and surface pore structures. A significant variation in tensile strength at the low loading (1 wt.%) into the PAI membrane. The experimental results confirmed that the physical and chemical properties of the PAI membrane were altered depending on the loading wt.% of ZIF-8 and CMS. Furthermore, the ZIF-8 nanocrystal is expected to offer an electrostatic field with the CO_2 quadrupole moment, resulting in increased CO_2 selectivity. From the results, it can be concluded, the fabricated PAI/ZIF-8 and PAI/CMS can be promising membrane materials for gas separation with appropriate permeation, permeability, and selectivity properties.

Declarations

Conflict of interests

The authors declare that they have no conflict of interest.

Ethics approval and consent to participate

Not applicable.

Consent for publication

Not applicable.

Availability of data and materials

Not applicable.

Funding

The authors did not receive support from any organization for the submitted work.

Authors' contributions:

B. Sasikumar: Conceptualization, data collection, analysis, and writing, Yohannan Subin Sabilon: Methodology, and validation, Arthanareeswaran Gangasalam: Resources, Supervision, Review & Editing.

References

Aditya Kiran S, Lukka Thuyavan Y, Arthanareeswaran G, et al (2016) Impact of graphene oxide embedded polyethersulfone membranes for the effective treatment of distillery effluent. Chem Eng J 286:528–537. https://doi.org/10.1016/j.cej.2015.10.091

Anastasiou S, Bhoria N, Pokhrel J, Karanikolos GN (2016) Metal organic framework mixed matrix membranes for CO2separation. Soc Pet Eng - Abu Dhabi Int Pet Exhib Conf 2016 2016-Janua: https://doi.org/10.2118/183264-ms

Aroon MA, Ismail AF, Matsuura T, Montazer-Rahmati MM (2010) Performance studies of mixed matrix membranes for gas separation: A review. Sep Purif Technol 75:229–242. https://doi.org/10.1016/j.seppur.2010.08.023

Cheng Y, Ying Y, Zhai L, et al (2019) Mixed matrix membranes containing MOF@COF hybrid fillers for efficient CO2/CH4 separation. J Memb Sci 573:97–106. https://doi.org/10.1016/j.memsci.2018.11.060

Chung TS, Jiang LY, Li Y, Kulprathipanja S (2007) Mixed matrix membranes (MMMs) comprising organic polymers with dispersed inorganic fillers for gas separation. Prog Polym Sci 32:483–507. https://doi.org/10.1016/j.progpolymsci.2007.01.008

Cravillon J, Nayuk R, Springer S, et al (2011) Controlling zeolitic imidazolate framework nano- and microcrystal formation: Insight into crystal growth by time-resolved in situ static light scattering. Chem Mater 23:2130–2141. https://doi.org/10.1021/cm103571y

Dai Y, Johnson JR, Karvan O, et al (2012) Ultem ®/ZIF-8 mixed matrix hollow fiber membranes for CO 2/N 2 separations. J Memb Sci 401–402:76–82. https://doi.org/10.1016/j.memsci.2012.01.044

El-Sheikh MA (2016) A novel photo-grafting of acrylamide onto carboxymethyl starch. 1. Utilization of CMS-g-PAAm in easy care finishing of cotton fabrics. Carbohydr Polym 152:105–118. https://doi.org/10.1016/j.carbpol.2016.06.088

Goh PS, Ismail AF, Sanip SM, et al (2011) Recent advances of inorganic fillers in mixed matrix membrane for gas separation. Sep Purif Technol 81:243–264. https://doi.org/10.1016/j.seppur.2011.07.042

Ismail AF, Goh PS, Sanip SM, Aziz M (2009) Transport and separation properties of carbon nanotube-mixed matrix membrane. Sep Purif Technol 70:12–26. https://doi.org/10.1016/j.seppur.2009.09.002

Keskin S, Sholl DS (2009) Assessment of a metal-organic framework membrane for gas separations using atomically detailed calculations: CO 2, CH 4, N 2, H 2 mixtures in MOF-5. Ind Eng Chem Res 48:914–922. https://doi.org/10.1021/ie8010885

Lei L, Pan F, Lindbråthen A, et al (2021) Carbon hollow fiber membranes for a molecular sieve with precise-cutoff ultramicropores for superior hydrogen separation. Nat Commun 12:. https://doi.org/10.1038/s41467-020-20628-9

Liu J, He J, Wang L, et al (2016) NiO-PTA supported on ZIF-8 as a highly effective catalyst for hydrocracking of Jatropha oil. Sci Rep 6:1–11. https://doi.org/10.1038/srep23667

Liu X, Li Y, Ban Y, et al (2013) Improvement of hydrothermal stability of zeolitic imidazolate frameworks. Chem Commun 49:9140–9142. https://doi.org/10.1039/c3cc45308a

Maya F, Palomino Cabello C, Clavijo S, et al (2015) Zeolitic imidazolate framework dispersions for the fast and highly efficient extraction of organic micropollutants. RSC Adv 5:28203–28210. https://doi.org/10.1039/c5ra01079a

Meshkat S, Kaliaguine S, Rodrigue D (2020) Comparison between ZIF-67 and ZIF-8 in Pebax ® MH-1657 mixed matrix membranes for CO 2 separation. Sep Purif Technol 235:116150. https://doi.org/10.1016/j.seppur.2019.116150

Nordin NAHM, Ismail AF, Mustafa A, et al (2015) Utilizing low ZIF-8 loading for an asymmetric PSf/ZIF-8 mixed matrix membrane for CO2/CH4 separation. RSC Adv 5:30206–30215. https://doi.org/10.1039/c5ra00567a

Ordoñez MJC, Balkus KJ, Ferraris JP, Musselman IH (2010) Molecular sieving realized with ZIF-8/Matrimid® mixed-matrix membranes. J Memb Sci 361:28–37. https://doi.org/10.1016/j.memsci.2010.06.017

Pan Y, Liu Y, Zeng G, et al (2011) Rapid synthesis of zeolitic imidazolate framework-8 (ZIF-8) nanocrystals in an aqueous system. Chem Commun 47:2071–2073. https://doi.org/10.1039/c0cc05002d

Rajesh S, Fauzi Ismail A, Mohan DR (2012) Structure-property interplay of poly(amide-imide) and TiO2 nanoparticles impregnated poly(ether-sulfone) asymmetric nanofiltration membranes. RSC Adv 2:6854–6870. https://doi.org/10.1039/c2ra20265d

Robeson LM (2008) The upper bound revisited. J Memb Sci 320:390–400. https://doi.org/10.1016/j.memsci.2008.04.030

Sasikumar B, Bisht S, Arthanareeswaran G, et al (2021) Performance of polysulfone hollow fiber membranes encompassing ZIF-8, SiO2/ZIF-8, and amine-modified SiO2/ZIF-8 nanofillers for CO2/CH4 and CO2/N2 gas separation. Sep Purif Technol 264:118471. https://doi.org/10.1016/j.seppur.2021.118471

Sorribas S, Zornoza B, Téllez C, Coronas J (2014) Mixed matrix membranes comprising silica-(ZIF-8) core-shell spheres with ordered meso-microporosity for natural- and bio-gas upgrading. J Memb Sci 452:184–192. https://doi.org/10.1016/j.memsci.2013.10.043

Taheri P, Raisi A (2021) CO2 -selective poly (ether-block-amide)/ polyethylene glycol composite blend membrane for CO 2 separation from gas mixtures. 38274–38291

Vu DQ, Koros WJ, Miller SJ (2002) High Pressure CO_2/CH_4 Separation using Carbon Molecular Sieve Hollow Fiber Membranes. Ind Eng Chem Res 41:367–380. https://doi.org/10.1021/ie010119w

Vu DQ, Koros WJ, Miller SJ (2003a) Effect of condensable impurity in CO2/CH4 gas feeds on performance of mixed matrix membranes using carbon molecular sieves. J Memb Sci 221:233–239. https://doi.org/10.1016/S0376-7388(03)00245-X

Vu DQ, Koros WJ, Miller SJ (2003b) Mixed matrix membranes using carbon molecular sieves I . Preparation and experimental results. 211:311–334

Vu DQ, Koros WJ, Miller SJ (2003c) Mixed matrix membranes using carbon molecular sieves II . Modeling permeation behavior. 211:335–348

Xie K, Fu Q, Qiao GG, Webley PA (2019) Recent progress on fabrication methods of polymeric thin film gas separation membranes for CO2 capture. J Memb Sci 572:38–60. https://doi.org/10.1016/j.memsci.2018.10.049

Zhang C, Dai Y, Johnson JR, et al (2012) High performance ZIF-8 / 6FDA-DAM mixed matrix membrane for propylene / propane separations. J Memb Sci 389:34–42. https://doi.org/10.1016/j.memsci.2011.10.003

Zhang C, Zhang K, Xu L, et al (2014) Highly Scalable ZIF-Based Mixed-Matrix Hollow Fiber Membranes for Advanced Hydrocarbon Separations. 60:. https://doi.org/10.1002/aic

Zhang Y, Sunarso J, Liu S, Wang R (2013) Current status and development of membranes for CO 2 / CH 4 separation : A review. Int J Greenh Gas Control 12:84–107. https://doi.org/10.1016/j.ijggc.2012.10.009

Figures

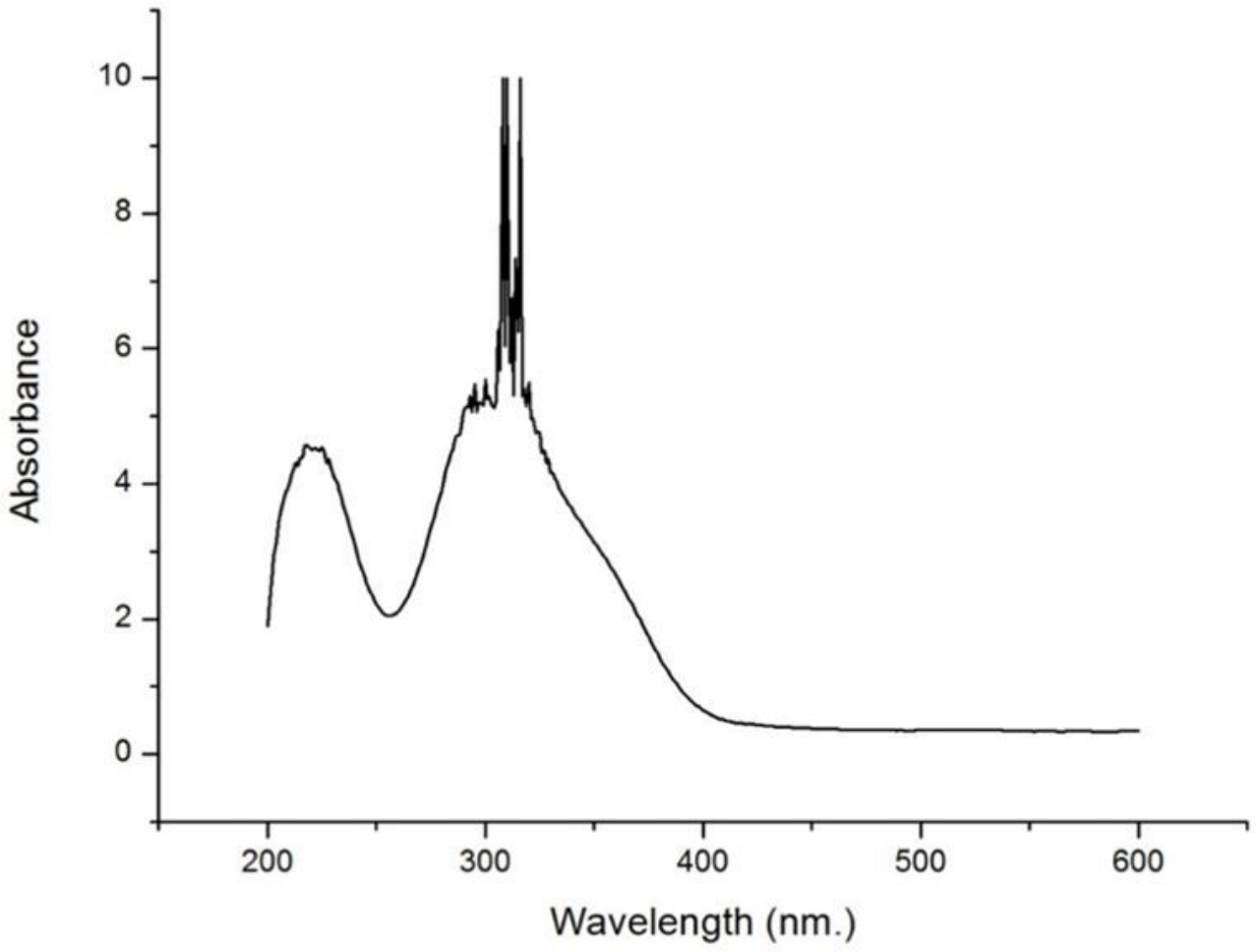

Figure 1

UV visible spectroscopy result of ZIF-8 nanocrystals

Figure 2

XRD spectra of ZIF-8 nanocrystals

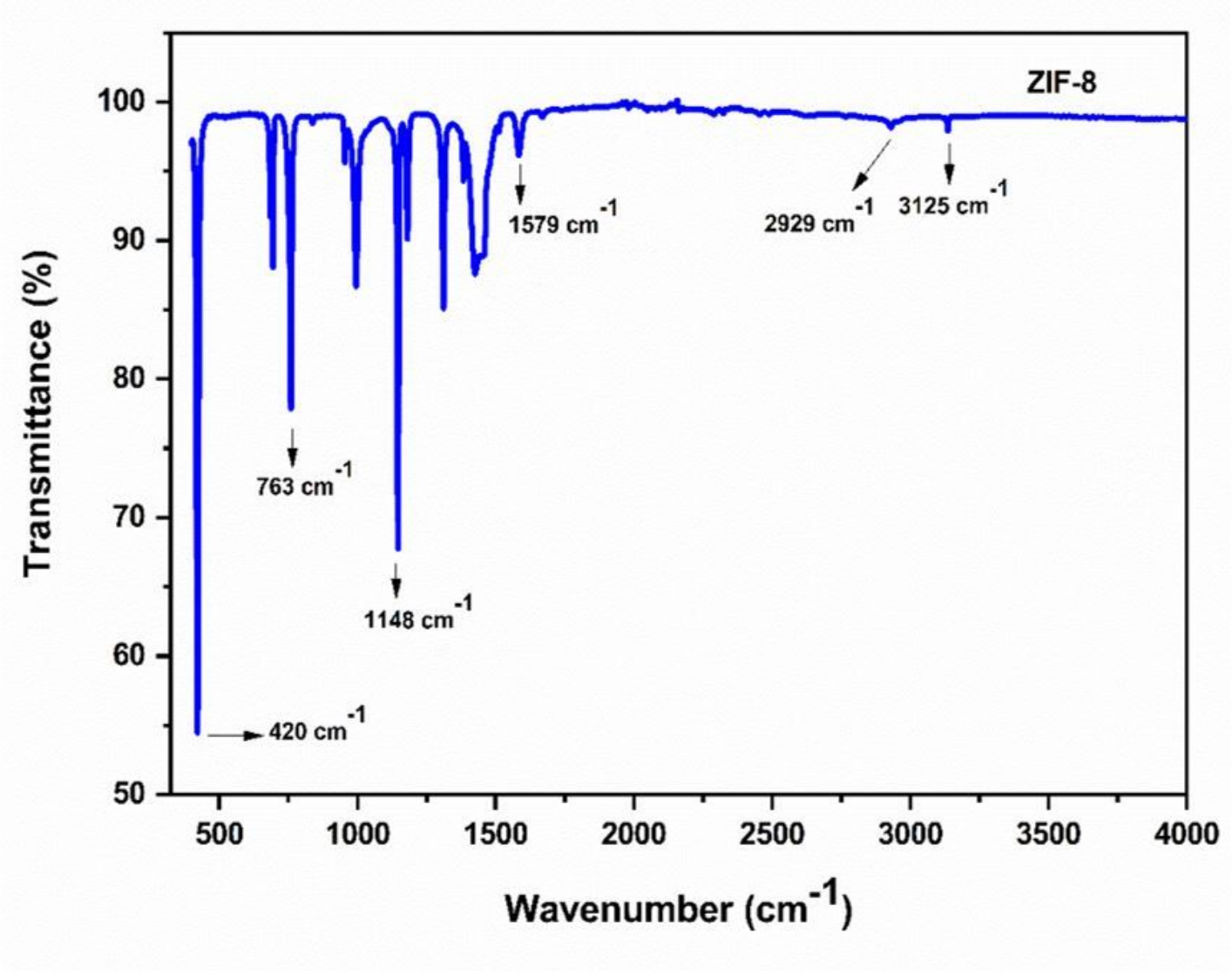

Figure 3

FTIR spectra of ZIF-8 nanoparticles

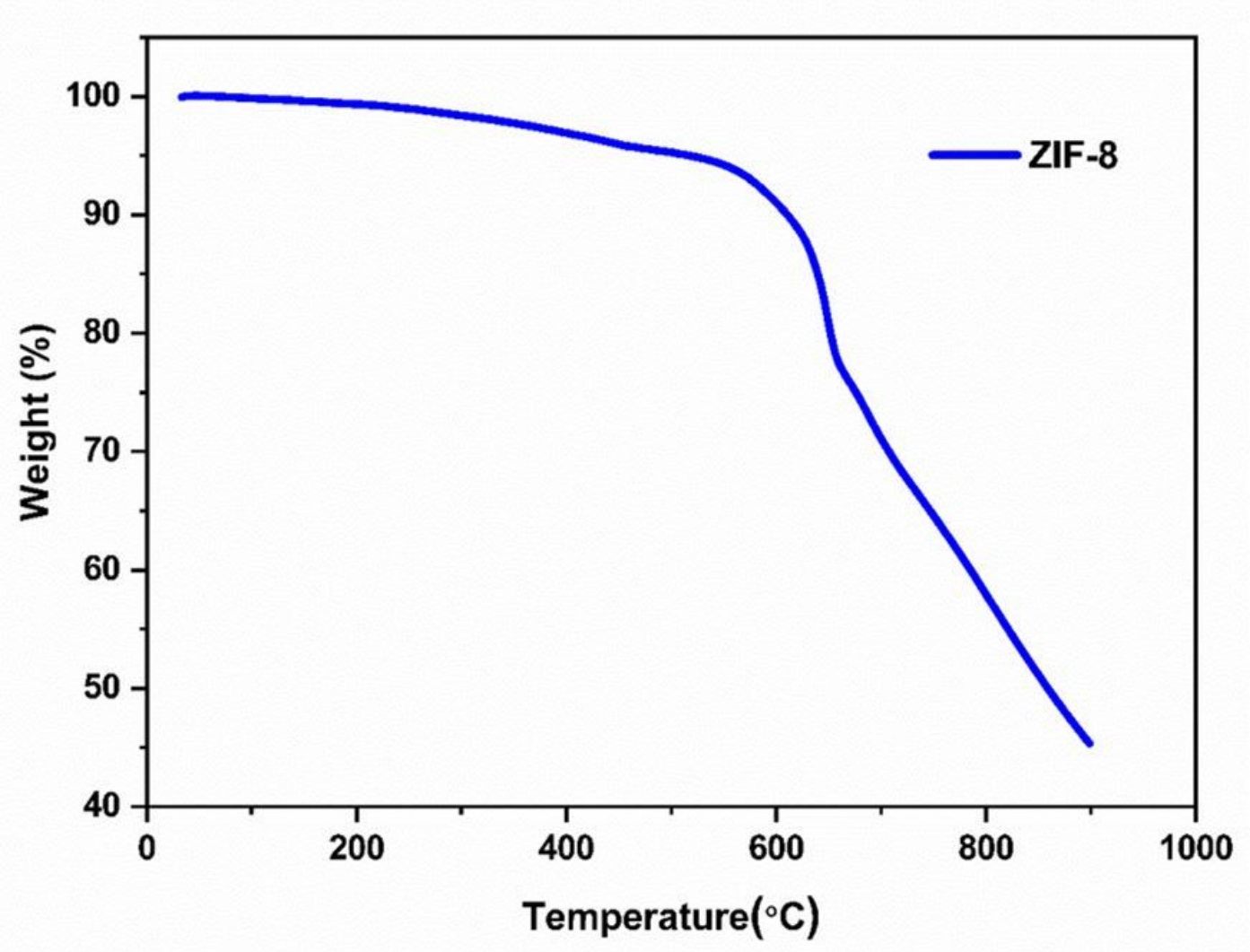

Figure 4

Thermal stability of ZIF-8 nanoparticles

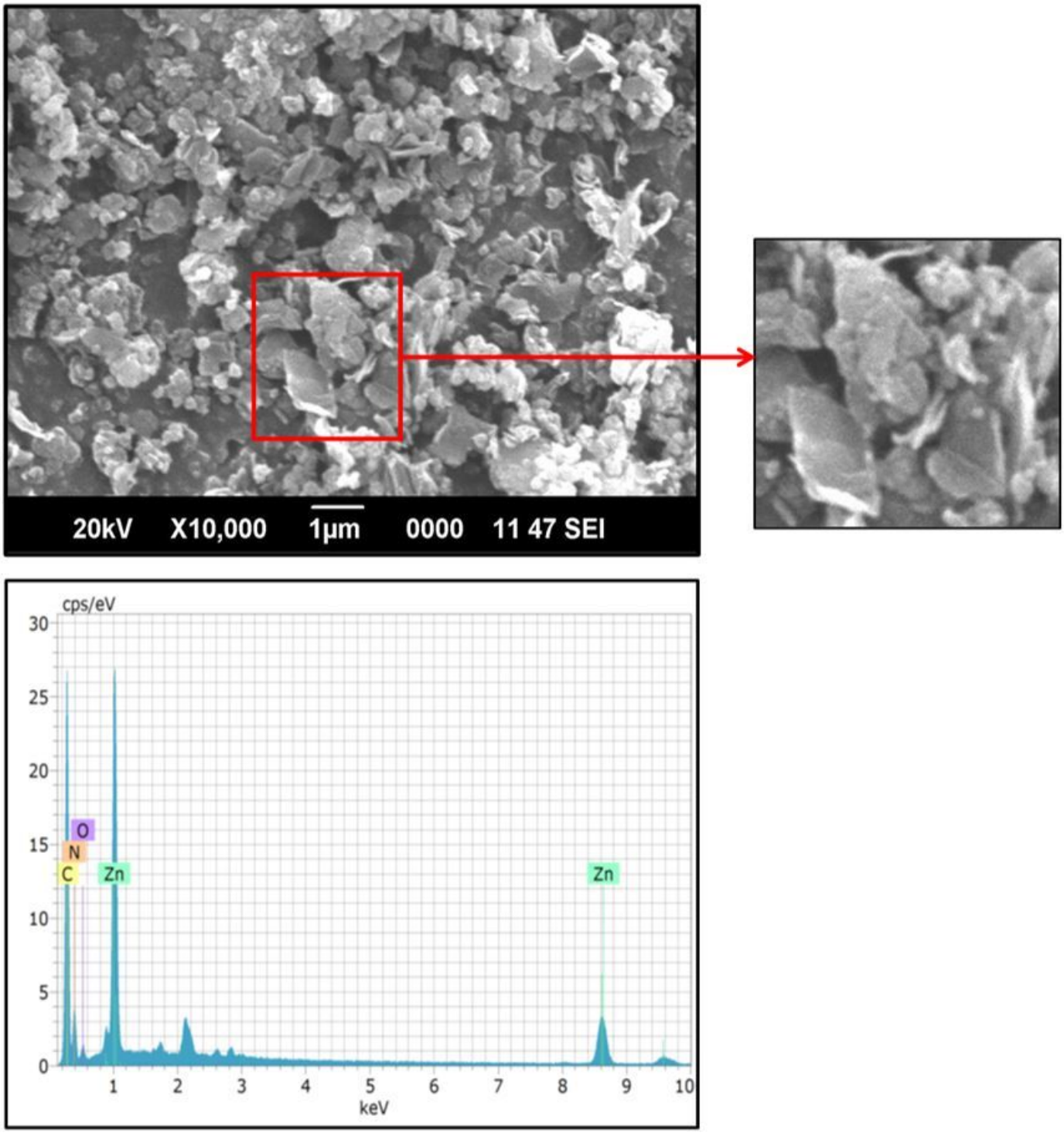

Figure 5

SEM-EDAX of ZIF-8 nanocrystals

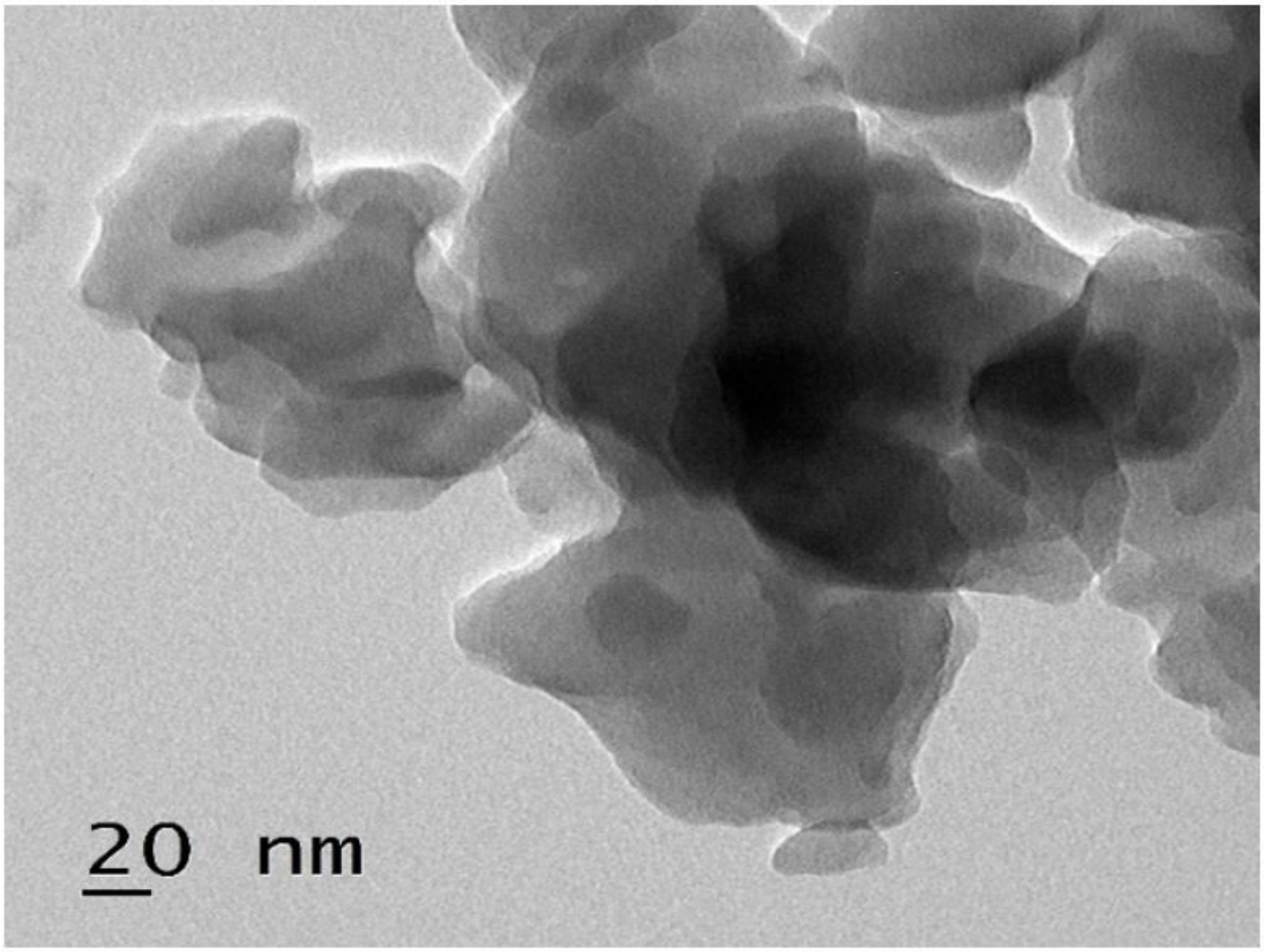

Figure 6

TEM image of ZIF-8 nanocrystals

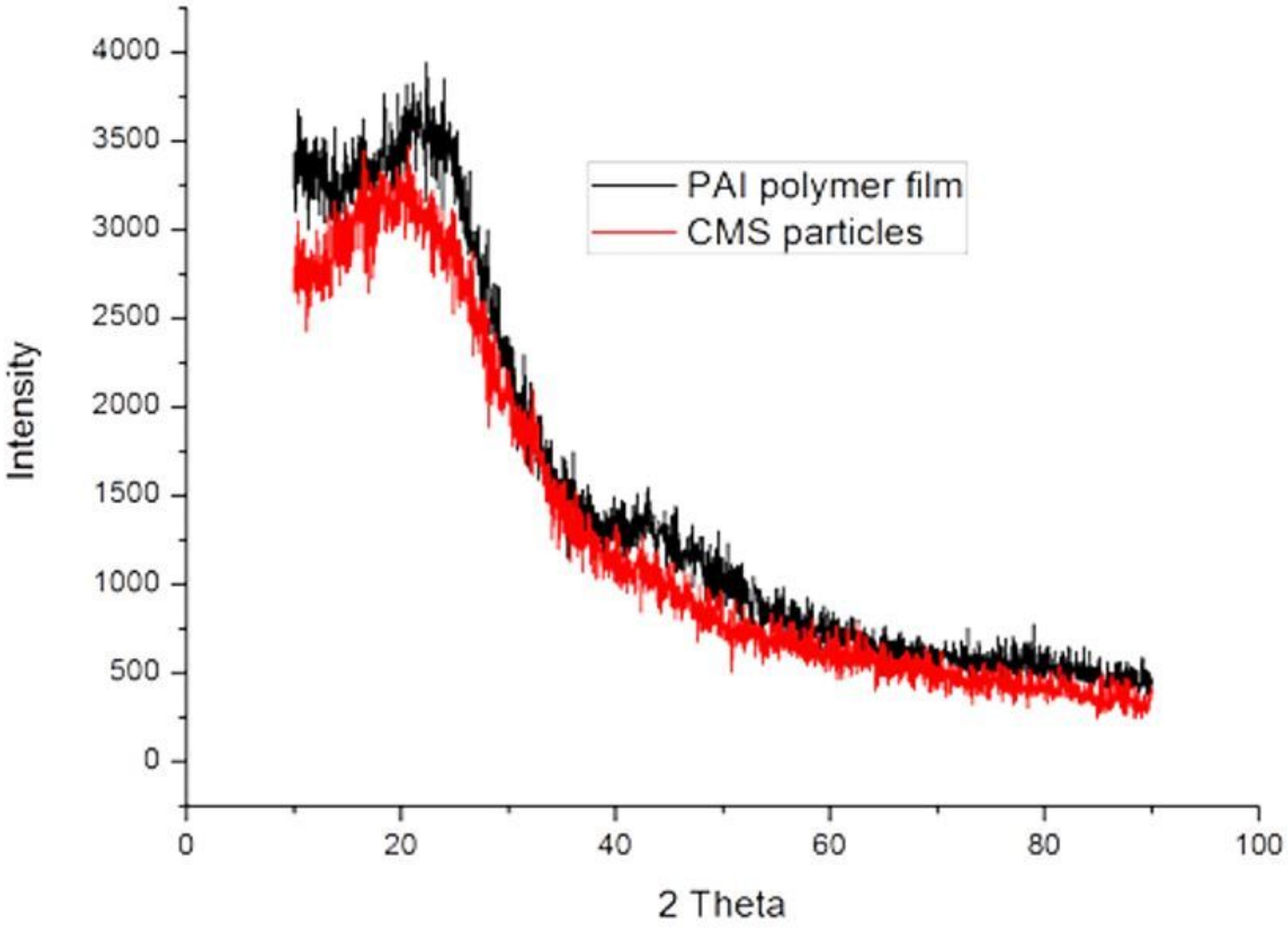

Figure 7

XRD results of CMS particles and CMS membrane

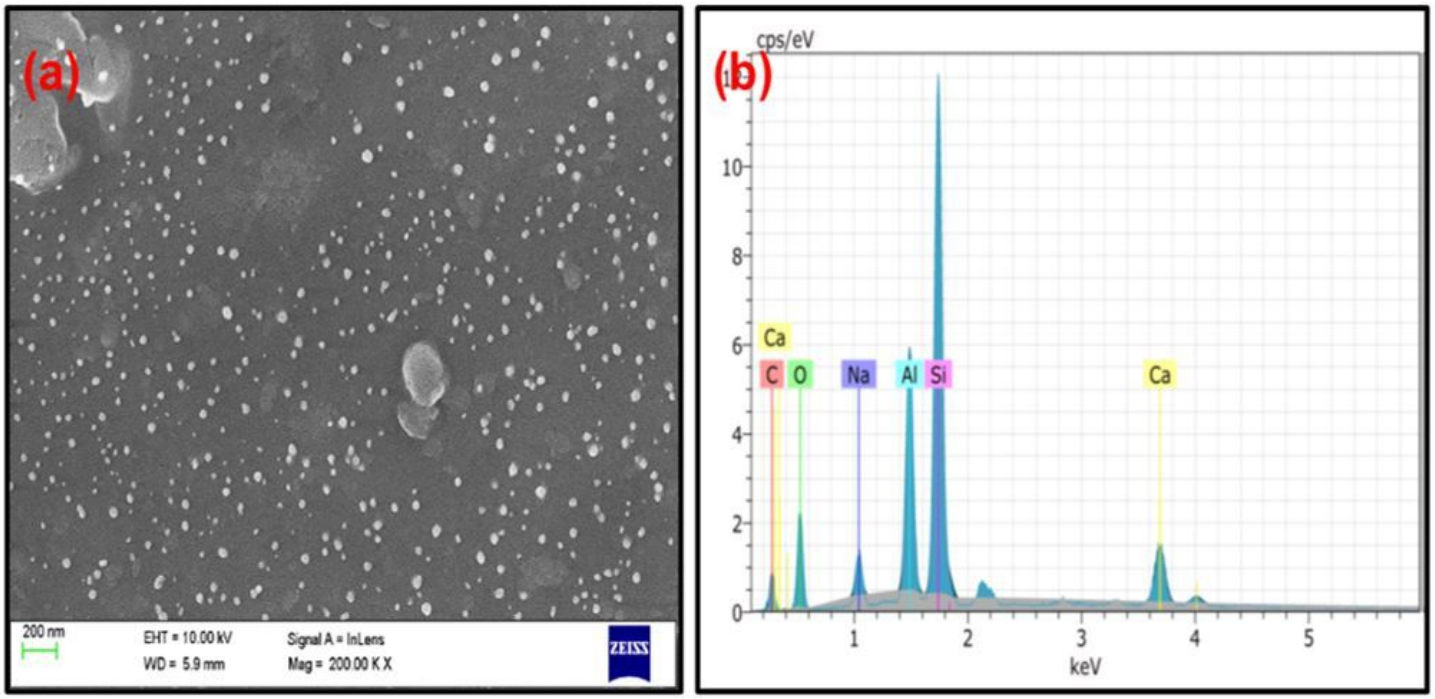

Figure 8

(a) Top surface morphology of PAI/CMS membrane (b) EDAX spectra of PAI/CMS membrane

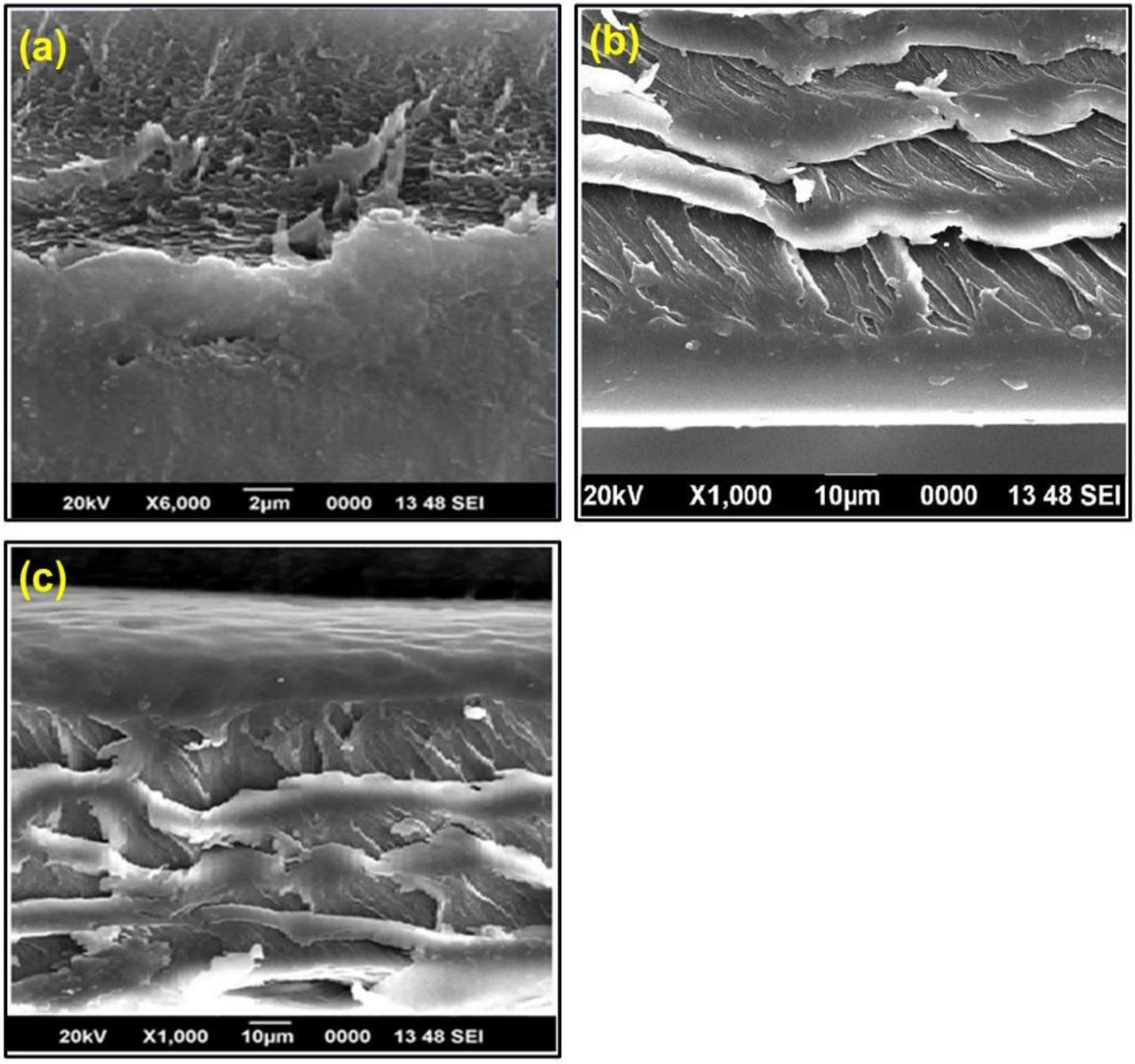

Figure 9

Cross-sectional morphology of (a) PAI/CMS (1%) (b) PAI/CMS (2%) (c) PAI/CMS (3%)

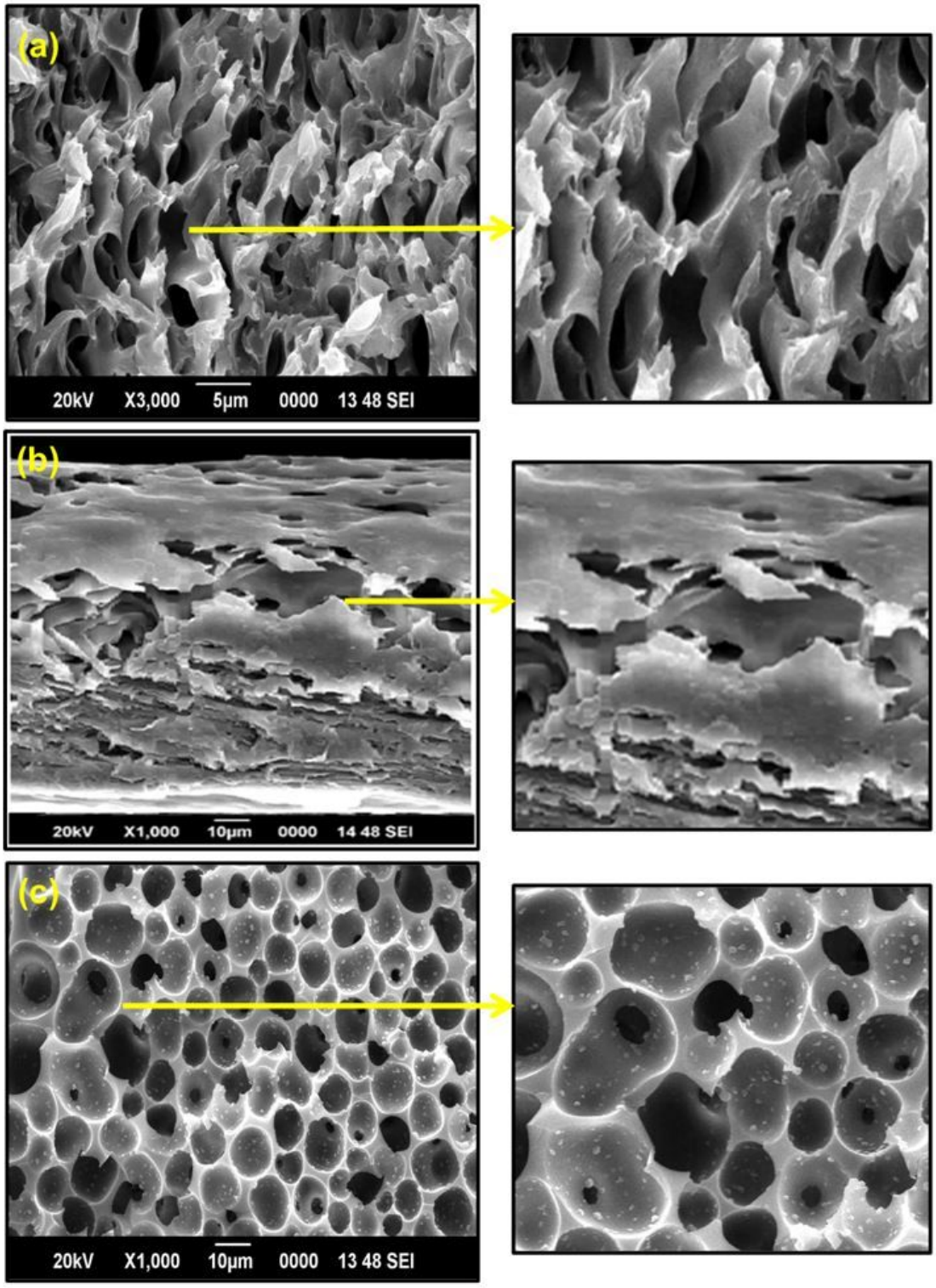

Figure 10

Cross-sectional morphology of (a) PAI/ZIF-8 (1%) (b) PAI/ZIF-8 (2%) (c) PAI/ZIF-8 (3%)

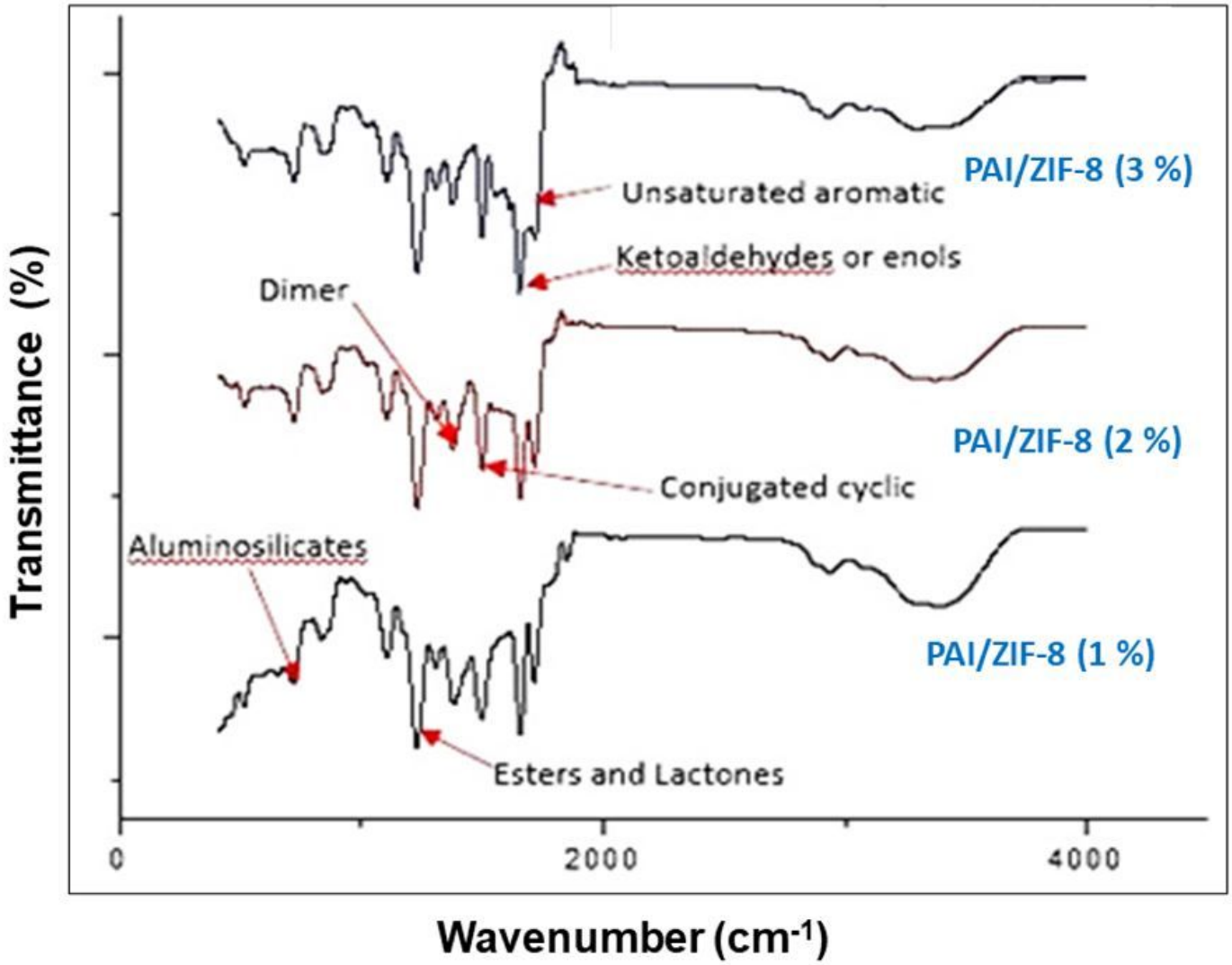

Figure 11

FTIR analysis of PAI/ZIF-8 membranes

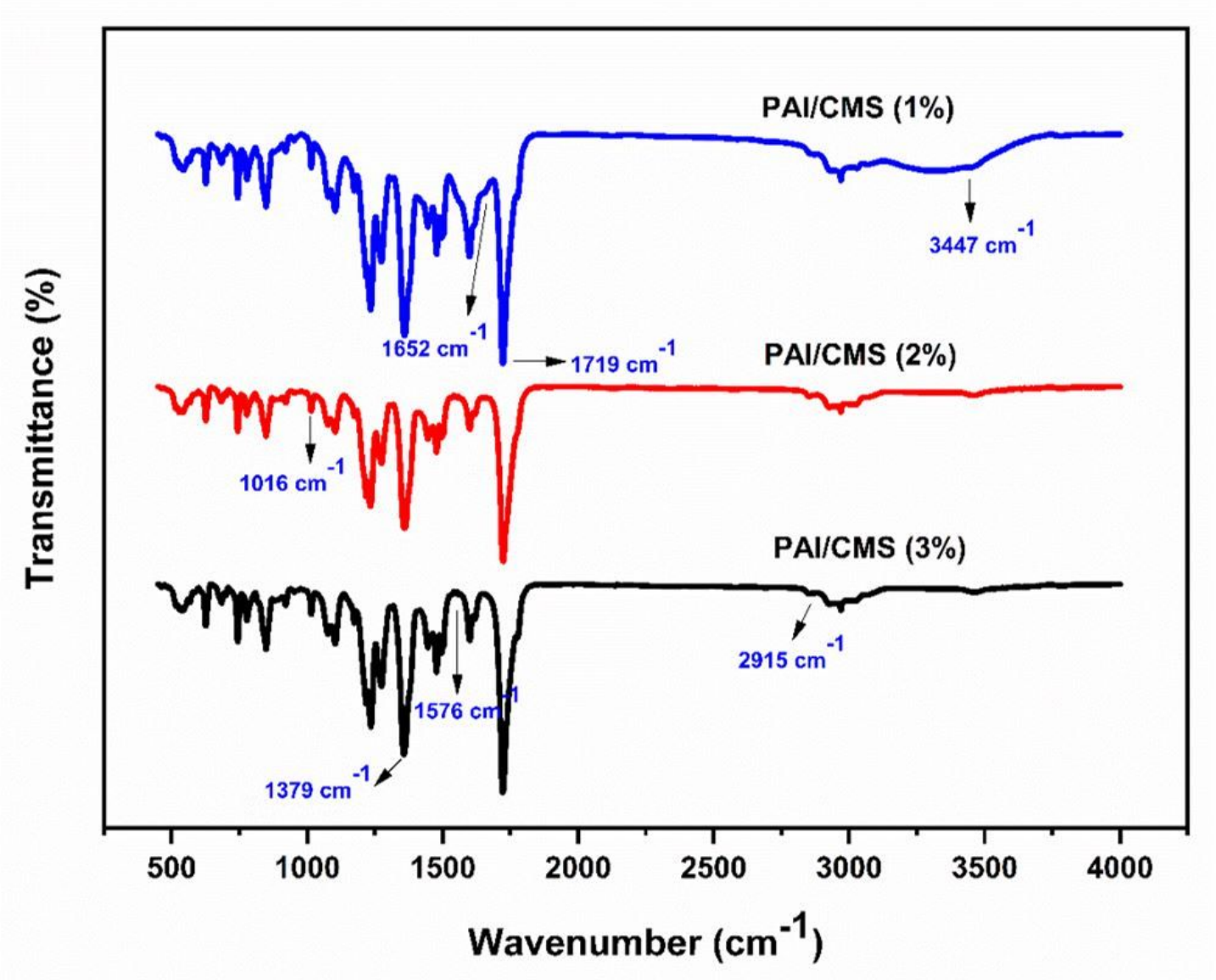

Figure 12

FTIR analysis of PAI/CMS membranes

Supplementary Files

This is a list of supplementary files associated with this preprint. Click to download.

- graphicsabstract.jpg
- Responsetoeditorcomments.pdf